



# Interannual variability of temperature in the UTLS region over Ganges–Brahmaputra–Meghna river basin based on COSMIC GNSS RO data

Khandu<sup>1</sup>, Joseph L. Awange<sup>1,2,3</sup>, and Ehsan Forootan<sup>4,5</sup>

<sup>1</sup>Department of Spatial Sciences, Curtin University, Perth, Australia

<sup>2</sup>Geodetic Institute, Karlsruhe University of Technology (KIT), Karlsruhe, Germany

<sup>3</sup>Department of Geophysics, Kyoto University, Kyoto, Japan

<sup>4</sup>Institute of Geodesy and Geoinformation, Bonn University, Bonn, Germany

<sup>5</sup>School of Earth and Ocean Sciences, Cardiff University, Cardiff, UK

Correspondence to: Khandu (khandu@postgrad.curtin.edu.au)

Received: 1 May 2015 – Published in Atmos. Meas. Tech. Discuss.: 14 September 2015

Revised: 25 March 2016 – Accepted: 29 March 2016 – Published: 15 April 2016

**Abstract.** Poor reliability of radiosonde records across South Asia imposes serious challenges in understanding the structure of upper-tropospheric and lower-stratospheric (UTLS) region. The Constellation Observing System for Meteorology, Ionosphere, and Climate (COSMIC) mission launched in April 2006 has overcome many observational limitations inherent in conventional atmospheric sounding instruments. This study examines the interannual variability of UTLS temperature over the Ganges–Brahmaputra–Meghna (GBM) river basin in South Asia using monthly averaged COSMIC radio occultation (RO) data, together with two global re-analyses. Comparisons between August 2006 and December 2013 indicate that MERRA (Modern-Era Retrospective Analysis for Research Application) and ERA-Interim (European Centre for Medium-Range Weather Forecasts reanalysis) are warmer than COSMIC RO data by 2 °C between 200 and 50 hPa levels. These warm biases with respect to COSMIC RO data are found to be consistent over time. The UTLS temperature show considerable interannual variability from 2006 to 2013 in addition to warming (cooling) trends in the troposphere (stratosphere). The cold (warm) anomalies in the upper troposphere (tropopause region) are found to be associated with warm ENSO (El Niño–Southern Oscillation) phase, while quasi-biennial oscillation (QBO) is negatively (positively) correlated with temperature anomalies at 70 hPa (50 hPa) level. PCA (principal component analysis) decomposition of tropopause temperatures and heights over

the basin indicate that ENSO accounts for 73 % of the inter-annual (non-seasonal) variability with a correlation of 0.77 with Niño3.4 index whereas the QBO explains about 10 % of the variability. The largest tropopause anomaly associated with ENSO occurs during the winter, when ENSO reaches its peak. The tropopause temperature (height) increased (decreased) by about 1.5 °C (300 m) during the last major El Niño event of 2009/2010. In general, we find decreasing (increasing) trend in tropopause temperature (height) between 2006 and 2013.

## 1 Introduction

The upper troposphere–lower stratosphere (UTLS) region (400–30 hPa) is characterized by steep changes in static stability (temperature lapse rate) with large gradients in a number of radiatively active trace gases, including ozone and water vapor (Reid and Gage, 1985; Randel et al., 2000). The variability and changes in UTLS temperature play an important role in regulating the exchange of water vapor, ozone, and other trace gases between the troposphere and the stratosphere. Observational evidence suggests that the troposphere has warmed considerably over the past decades with substantial cooling in the lower stratosphere (Karl et al., 2006; Lott et al., 2013; Thorne et al., 2013). Much of these temperature changes has been attributed to the increasing concentra-

tion of the greenhouse gases and are consistent with trends from climate model simulations (e.g., Lott et al., 2013; Santer et al., 2008). The *tropopause*, which marks the separation between the troposphere and the stratosphere in the UTLS region, is of special importance for understanding the transport of water vapor into the stratosphere and exchange of ozone between the two layers (Randel et al., 2000). The height of the tropopause is affected by the heat balance of both the troposphere (e.g., warming as a result of increasing greenhouse gas concentration) and the stratosphere (e.g., warming as a result of absorption of aerosols) (Santer et al., 2003a, b, 2008).

Many studies have analyzed the seasonal and interannual variations of UTLS temperature using observations from global network of radiosondes, satellite-based measurements, and global reanalyses (e.g., Reid and Gage, 1985; Randel et al., 2000; Gettelman et al., 2001; Santer et al., 2003a, b; Wilcox et al., 2011; Lott et al., 2013). Large-scale variation of the tropopause is dominated by an annual cycle and longer-term interannual variability associated with the El Niño–Southern Oscillation (ENSO; Trenberth, 1990) and the quasi-biennial oscillation (QBO; Baldwin et al., 2001). While the global characteristics of UTLS temperature is widely studied, much remains to be known in terms of its regional behavior and how it influences the regional climate (e.g., rainfall). Large observational uncertainties still exist over South Asia, specifically over the Ganges–Brahmaputra–Meghna (GBM) river basin due to poor quality of radiosonde networks (e.g., Das Gupta et al., 2005; Sun et al., 2010; Kumar et al., 2011; Ansari et al., 2015). Some stations have been recently updated by the Indian Meteorological Department (IMD) with Global Positioning System (GPS)-based radiosondes to improve their accuracy (see Kumar et al., 2011; Ansari et al., 2015). Our analysis over the GBM basin between August 2006 and December 2013 shows that GPS-based radiosondes have been significantly improved over the previous versions and exhibit negligible bias against the highly accurate Constellation Observing System for Meteorology, Ionosphere, and Climate (COSMIC; Anthes et al., 2008) radio occultation (RO) data sets.

The GBM river basin is located in a region where the UTLS is characterized by large-scale anticyclonic circulation that is dynamically active and coupled to the Indian monsoon circulation (Rao et al., 2008; Kunze et al., 2010). As a dominant source of seasonal and interannual variability, the Indian monsoon is also a major source of moisture in the UTLS as well as an important mode of transport for many trace gases and other pollutants over the region. The temperature changes in the UTLS affects static stability (e.g., increase with respect to global warming) with the potential to alter global and region weather/climate. The recent weakening of the Indian monsoon has been attributed to the upper-tropospheric cooling (warming) over the anticyclonic region (equatorial Indian Ocean) (Rao et al., 2008; Kunze et al., 2010). With increasing population and rapid industrializa-

tion, the GBM river basin has witnessed a dramatic increase in atmospheric pollution and aerosols that has been found to influence rainfall patterns (Gautam et al., 2009; Lau et al., 2009).

Since the launch of GPS/Meteorology (GPS/MET) mission in 1995 (Rocken et al., 1997), Global Navigation Satellite Systems (GNSS) RO has demonstrated immense potential to provide improved spatio-temporal (and vertical) resolution in the probing of the Earth's atmosphere including pressure, temperature, and water vapor (Schmidt et al., 2010; Anthes, 2011). Several studies have demonstrated the usefulness of GNSS RO in improving numerical weather prediction forecasts (e.g., Healy and Thépaut, 2006; Cucurull et al., 2007; Poli et al., 2008, 2010), climate studies (Foelsche et al., 2008; Schmidt et al., 2010; Steiner et al., 2013), and space weather/ionospheric research and operations (e.g., Lee et al., 2012; Zhang et al., 2014) over the past 2 decades. The number of RO profiles has increased substantially over the past years with the launch of several GNSS RO missions enabling wider applications in regional studies (see, e.g., Anthes, 2011). For instance, the joint Taiwan–US six-satellite mission, COSMIC/FORMOSA Satellite Mission 3 (COSMIC/FORMOSAT-3, hereafter COSMIC) (Anthes et al., 2008), has provided about 1500–2000 RO soundings per day globally with 70–90 % of the soundings since August 2006. It is now possible to infer decadal temperature trends in the UTLS and the tropopause with a structural uncertainty of less than 0.06 °C in the tropics and mid-latitudes (Steiner et al., 2013). Using ~ 9 years of RO data from CHALLENGING Minisatellite Payload (CHAMP, 2001–2008 Wickert et al., 2001), Gravity Recovery And Climate Experiment (GRACE, 2006–2009 Wickert et al., 2009), and COSMIC (2006–2009), Schmidt et al. (2010) found an increase of global tropopause height (5–9 m year<sup>-1</sup>), which is consistent with the current global warming trends.

In the context of growing RO mission and its ability to provide high spatio-temporal (and vertical) resolution vertical profiles, this study examines the interannual variability of temperature in the UTLS over the GBM river basin using ~ 8 years of monthly accumulated COSMIC RO data from August 2006 to December 2013. Two global reanalysis fields from European Centre for Medium-Range Weather Forecasts reanalysis (ERA-Interim; Dee et al., 2011) and Modern-Era Retrospective Analysis for Research Application (MERRA; Rienecker et al., 2011) are also used in conjunction with COSMIC RO data to examine their accuracies over the region. Reanalyses have proven to be useful in understanding the thermodynamics of the lower atmosphere as well as the tropospheric–stratospheric exchange process. Both ERA-Interim and MERRA were developed primarily to improve on various aspects of the hydrologic cycle that were not adequately represented in previous generations of reanalyses (Dee et al., 2011; Rienecker et al., 2011). ERA-Interim also assimilates refractivity profiles from various GNSS RO missions from 2001 to reduce temperature biases (Poli et al.,

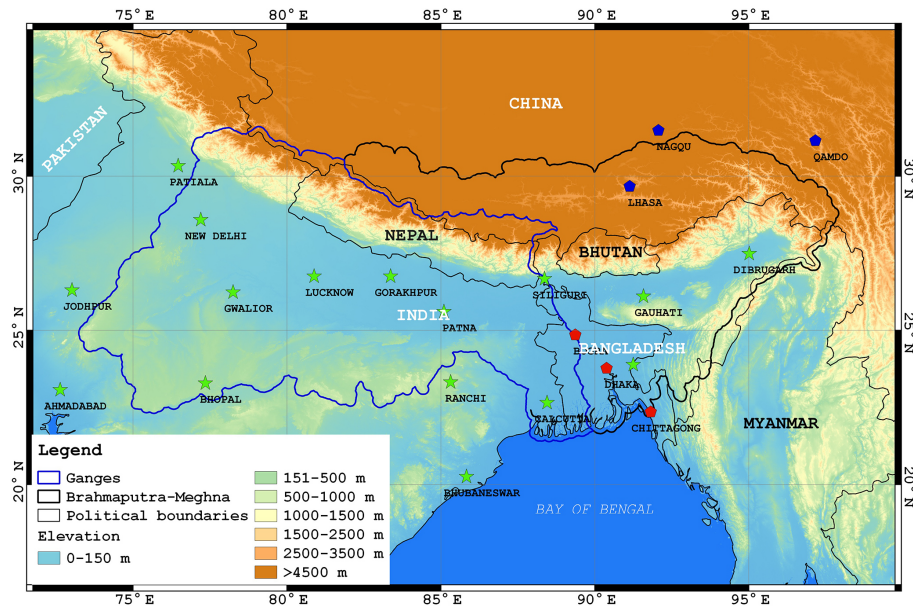


**Figure 1.** Overview of the GBM basin in South Asia. The digital elevation model displayed is derived from the Shuttle Radar Topography mission (SRTM, <http://srtm.csi.cgiar.org>). The locations of the radiosonde stations are shown in different colors, green for those over India (IMD/MK4), red for those over Bangladesh (unknown), and blue for those over China (ShangE/M), and their details are shown in Table S1 in the Supplement.

2010; Dee et al., 2011). Thus, modern reanalyses such as MERRA and ERA-Interim are expected to accurately capture the interannual variability of temperature in the UTLS for the most recent decade.

The remainder of the study is organized as follows. In Sect. 2, the study region is presented. This is followed in Sect. 3 by the description of data sets and methods used. The results are presented and discussed in Sect. 4, and Sect. 5 concludes the study.

## 2 GBM river basin

The GBM river basin in South Asia is a combination of three large river basins, namely the Ganges basin (907 000 km<sup>2</sup>), Brahmaputra basin (583 000 km<sup>2</sup>), and the Meghna basin (65 000 km<sup>2</sup>) (Chowdhury and Ward, 2004). Figure 1 shows an overview of the GBM river basin, which is being shared by five countries: India (64 %), China (18 %), Nepal (9 %), Bangladesh (7 %), and Bhutan (3 %). The GBM river basin, with a total surface area of approximately 1.75 million km<sup>2</sup> and an elevation range of about 8000 m, features distinct climatic characteristics owing to factors such as high topographic variations, the Indian Monsoon, and its interaction with large-scale circulations (e.g., Chowdhury, 2003). For example, Ganges basin is generally characterized by low precipitation whereas the Brahmaputra and Meghna basins are characterized by high rainfall amount (Mirza et al., 1998) during the summer. The Himalayan fronts (e.g., Meghalaya Plateau) act as a barrier to the monsoon flow and are usu-

ally characterized by pronounced rainfall especially during the summer.

The atmospheric conditions over the basin are largely controlled by the monsoon circulation during the summer, which is often modulated by global and regional large-scale climate variabilities such as ENSO and Indian Ocean Dipole (IOD) (e.g., Chowdhury, 2003; Ashok and Saji, 2007). The impact of global warming, increasing population, and rapid industrial and agricultural activities, and land-use changes across the basin may have contributed significantly to the recent tropospheric warming (Gautam et al., 2009; Lau et al., 2009).

## 3 Data and methods

### 3.1 FORMOSAT/COSMIC RO data

COSMIC is a highly successful RO mission that has demonstrated wide scientific applications in operational weather forecasts (see, e.g., Anthes et al., 2008; Ho et al., 2010; Anthes, 2011) and global atmospheric studies (see, e.g., Foelsche et al., 2008; Schmidt et al., 2010). In the RO data retrieval process, the bending angle ( $\alpha$ ) derived from Doppler shift measurements onboard low earth orbiting (LEO) satellites can be inverted to recover refractivity ( $N$ ) based on the Abel transform, which is related to total pressure ( $P$ ), temperature ( $T$ ), and water vapor pressure ( $P_w$ ) (Melbourne et al., 1994). In a dry atmosphere (with  $P_w = 0$ ), density profiles are obtained from the known relationship between refractivity and density, while pressure and dry temperature

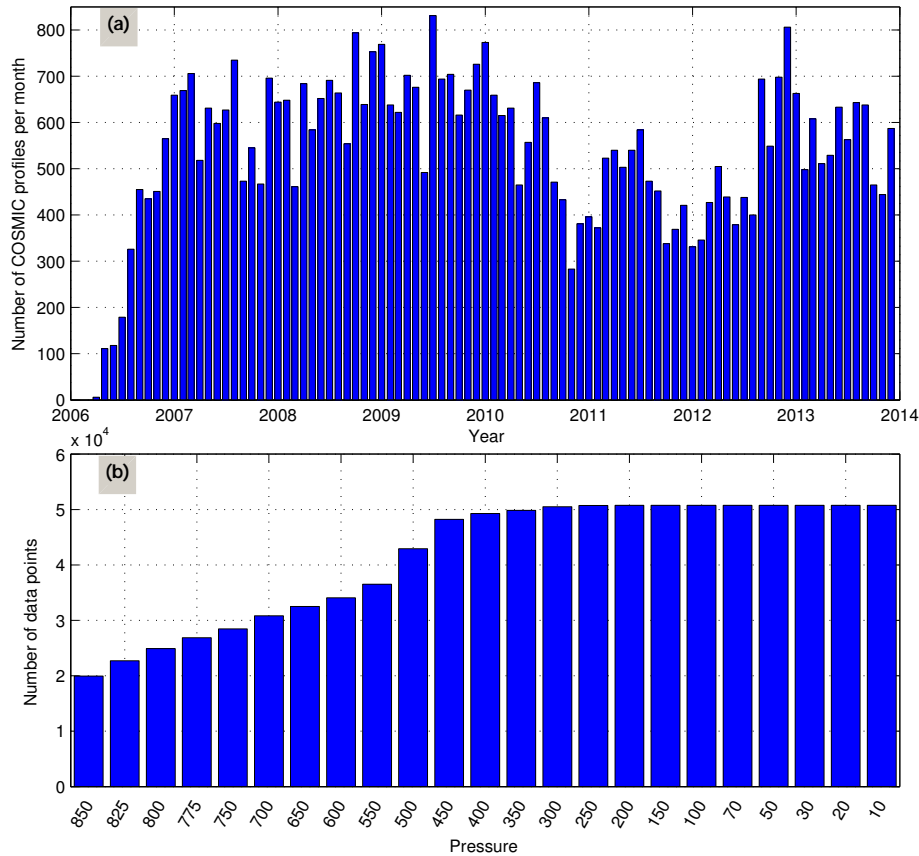


**Figure 2.** (a) Total number of monthly COSMIC RO profiles reported in and around the GBM river basin between April 2006 and December 2013, and (b) the corresponding number of data points at each pressure levels 850–30 hPa (1.5–24.0 km).

can be derived using the hydrostatic equation and equation of state for ideal gas (see Melbourne et al., 1994). In the presence of water vapor (especially in the lower troposphere), humidity and temperature profiles should be complemented with a priori information (e.g., numerical weather forecasts).

Alternatively, wet profiles can be generated using a one-dimensional variational (1-D-Var) method implemented at the COSMIC Data Analysis and Archive Center (CDAAC) at the University Corporation for Atmospheric Research (UCAR). These atmospheric profiles are provided as Level 2 RO data by various data retrieval centers including CDAAC (see <http://cdaac-www.cosmic.ucar.edu/cdaac/status.html>). In this study, COSMIC Level 2 RO data (both wet and dry profiles) covering the GBM river basin between April 2006 and December 2013 are used. The wet and dry profiles mainly differ in the lower troposphere due to presence of water vapor but are similar and highly accurate between 8 and 20 km (see Anthes et al., 2008). The wet profiles are used for evaluating the accuracy of radiosonde observations (see details in Supplement) while the dry profiles (i.e., temperature only) are used for examining the interannual variations of UTLS over the GBM river basin. The GBM river basin received 59 419 COSMIC profiles from

April 2006 to December 2013, out of which  $\sim 14\%$  were found to be of bad quality. Figure 2a shows the number of monthly accumulated COSMIC RO data retrieved during the period, which indicated an average of  $\sim 576$  profiles per month. The number of profiles decreased considerably between late 2010 and 2012 (Fig. 2a) due to problems in some COSMIC satellites (see <http://cdaac-www.cosmic.ucar.edu/cdaac/status.html>). Figure 2b shows the distribution of RO data points at various pressure (altitude) levels indicating that many COSMIC data penetrate deep into the lower troposphere with more than 56% of the profiles reaching at least 850 hPa ( $\sim 1.5$  km a.m.s.l.). The geographical distribution of COSMIC profiles at 850 hPa ( $\sim 1.5$  km), 700 hPa ( $\sim 3.1$  km), 500 hPa ( $\sim 6.0$  km), and 400 hPa ( $\sim 7.5$  km) levels in Fig. 3a–d indicates the effect of high topography over the region (Fig. 1), which blocks the GNSS radio waves. A near-complete coverage of the RO data can be seen at 400 hPa ( $\sim 7.5$  km), corresponding to the highest altitude of the Himalayas.

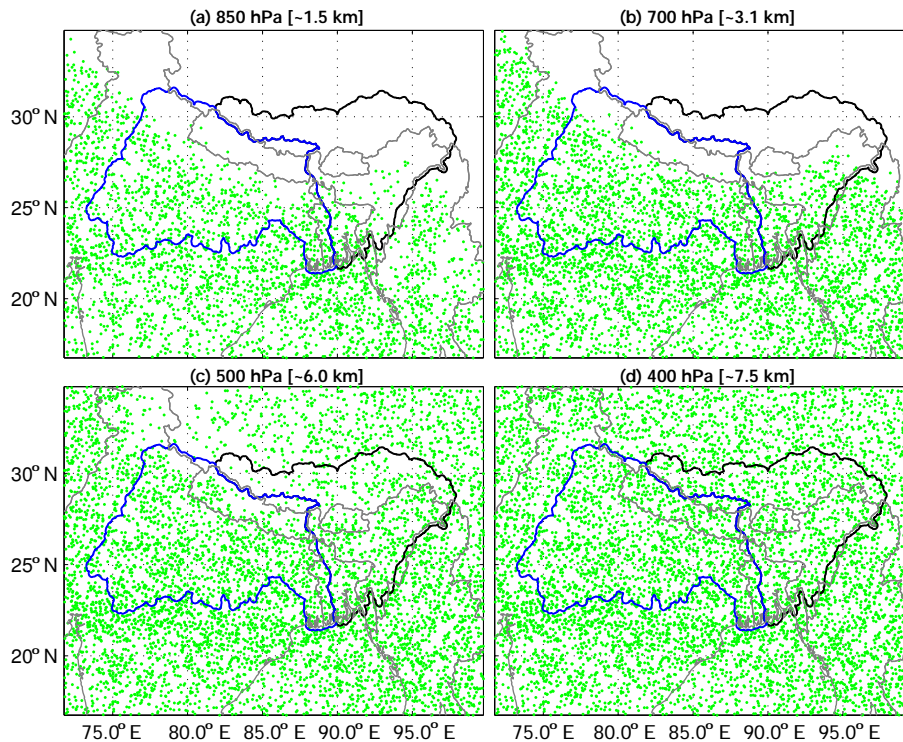


**Figure 3.** (a) Spatial distribution of COSMIC data points in the lower troposphere for the year 2012: (a) 850 hPa ( $\sim 1.5$  km), (b) 700 hPa ( $\sim 3.1$  km), (c) 500 hPa ( $\sim 5.8$  km), and (d) 400 hPa ( $\sim 7.5$  km).

### 3.2 Reanalysis products

COSMIC temperature profiles over the GBM region are compared with two high-resolution modern reanalysis products, (a) MERRA (Rienecker et al., 2008) and (b) ERA-Interim (Dee et al., 2011). MERRA is produced by the state-of-the-art Goddard Earth Observing System Data Assimilation System version 5 (GOES-5), at National Aeronautic and Space Administration (NASA), USA. GEOS-5 assimilates data from a wide variety of observing systems (e.g., in situ, satellites) to produce a consistent set of spatio-temporal meteorological and climatic variables since the start of the satellite era (i.e., 1979). GEOS-5 is run on a  $1/2^\circ \times 2/3^\circ$  (or  $\sim 50 \times 70$  km) grid with 72 vertical layers extending from the surface through to the stratosphere. Atmospheric variables (e.g., temperature, humidity) are produced at various temporal scales ranging from 3 hourly at  $1.5^\circ \times 1.5^\circ$  (or  $\sim 150 \times 150$  km grid) to monthly scales at the nominal horizontal resolution.

ERA-Interim is the latest global atmospheric reanalysis produced by ECMWF covering the period 1979 to present (Dee et al., 2011). ERA-Interim builds on the previous generation of reanalyses (e.g., ERA-15 and ERA-40) with improved model aspects, more advanced assimilation techniques (e.g., 4-D Variational Schemes) and better land surface model, and assimilates atmospheric profiles retrieved from the GNSS RO data. The atmo-

spheric variables (e.g., temperature and water vapor) are simulated at 6-hourly timescales over 60 vertical levels at a  $\sim 79 \times \sim 79$  km grid. Because ERA-Interim assimilates GNSS RO data, ERA-Interim and COSMIC RO data are not completely independent. Poli et al. (2010) found that GNSS RO data help to reduce temperature bias of ERA-Interim in the UTLS but are found to produce drying effects in the tropics. Monthly mean temperatures at 14 pressure levels from 500 to 10 hPa are obtained for both MERRA (see <http://disc.sci.gsfc.nasa.gov/daac-bin/FTPSubset.pl>) and ERA-Interim (see <http://apps.ecmwf.int/datasets/data/interim-full-daily/levtype=sfc/>) to assess UTLS temperature over the GBM river basin.

### 3.3 Ocean–atmospheric indices

Three ocean–atmospheric indices are used in this study, representing the (a) ENSO, (b) IOD, and (c) QBO, which are commonly associated with significant fluctuations in UTLS temperatures. ENSO is commonly defined by sea surface temperature (SST) anomalies in the equatorial Pacific ocean, typically over  $5^\circ \text{N}–5^\circ \text{S}$ ,  $120–170^\circ \text{W}$ , which is also known as Niño3.4 region (see Trenberth, 1990). ENSO events are said to occur if SST anomalies exceed  $4^\circ \text{C}$  for 6 months or more. Warm and cold ENSO phases are referred to as El Niño and La Niña events, respectively, which are represented by anomalous warming of the central and eastern

tropical Pacific (warm phase) and vice versa. Niño3.4 index is obtained from the National Oceanic and Atmospheric Administration (NOAA, see <http://www.esrl.noaa.gov/psd/data/climateindices/list/>).

IOD is measured by difference of SST anomalies between the western (50–70° E and 10° S–10° N) and eastern (90–110° E and 10–0° S) equatorial Indian ocean, also referred to as Dipole Mode Index (DMI). Positive IOD events are identified by cooler than normal water in the tropical eastern Indian Ocean and warmer than normal water in the tropical western Indian Ocean and are associated with a shift of active convection from eastern Indian Ocean to the west, leading to potentially higher than normal rainfall over parts of the Indian subcontinent. DMI is obtained from <http://www.jamstec.go.jp/frsgc/research/d1/iod/>. QBO is stratospheric phenomenon characterized by an east–west oscillation in stratospheric winds over a period of approximately 28 months (Baldwin et al., 2001). The QBO dominates variability of the equatorial stratosphere and is easily identified as downward propagating easterly (negative) and westerly (negative) wind regimes. It is commonly characterized by an index derived based on zonal winds at 30 or 50 hPa. Here, the QBO index at 30 hPa level covering the period 2006–2013 is obtained from NOAA (<http://www.esrl.noaa.gov/psd/data/correlation/qbo.data>).

### 3.4 Tropopause temperatures and heights

Various methods have been used to define the tropopause, such as lapse-rate tropopause (LRT), cold point tropopause, dynamical tropopause (isentropic potential vorticity), ozone tropopause, and 100 hPa pressure level (see Pan et al., 2004). This study focuses on the changes and interannual variations of the LRT given that it is an important indicator of climate change (see Santer et al., 2003a; Sausen and Santer, 2003). Based on WMO (1957), the LRT (hereinafter as tropopause) is defined as “the lowest level at which the lapse rate decreases to 2° km<sup>-1</sup> or less, provided also the average lapse rate between this level and all higher levels within 2 km does not exceed 2° C km<sup>-1</sup>”. COSMIC RO data obtained from CDAAC already contain the derived tropopause parameters (heights and temperatures), while MERRA also provides tropopause temperatures and pressures based on the WMO (1957) definition. The tropopause heights,  $h_{\text{LRT}}$  (in km), for MERRA was approximated from the tropopause pressures,  $P$  (in Pa), using the following relationship (PSAS, 2004):

$$h_{\text{LRT}} \equiv 44\,330.8 - 4946.54 \times P^{0.1902632}. \quad (1)$$

### 3.5 Principal component analysis (PCA)

Monthly COSMIC RO data are interpolated to a 0.5° × 0.5° grid over 14 standard pressure levels from 500 to 10 hPa (or 7.5–31 km) and the tropopause using the kriging technique (see details in the Supplement). Geostatistical kriging methods have been shown to be more robust and spatially more

reliable than other existing methods such as inverse distance weighting, Thiessen polygons (see, e.g., Goovaerts, 2000). To study the interannual variations of temperature at various pressure levels, PCA (Preisendorfer, 1988) is applied to the deseasonalized (annual cycle removed) tropopause heights and temperatures. PCA is a well-known data exploratory tool used in atmospheric/oceanic science since it allows for a space–time display of geophysical data (e.g., temperature), in very few modes (see Randel et al., 2000; Gettelman et al., 2001). The idea of PCA is to find a set of orthogonal spatial patterns (or empirical orthogonal functions, EOFs) along with a set of associated uncorrelated time series or principal components (PCs) that captures most of the observed variance (expressed in percent) from the available spatio-temporal data (e.g., temperature). In summary, the EOF decomposition can be written as  $\mathbf{X}_{(t,s)} = \mathbf{P}_{(t,n)} \mathbf{E}_{(s,n)}^T$ , where  $\mathbf{X}_{(t,s)}$  is the space ( $s$ )–time ( $t$ ) data with time mean or annual cycle removed,  $\mathbf{E}_{(s,n)}$  contains the EOFs with  $n$  number of retained modes, and  $\mathbf{P}_{(t,n)}$  are the PCs obtained by projecting the original data ( $\mathbf{X}_{(t,s)}$ ) on the orthogonal base functions  $\mathbf{E}_{(s,n)}$ , i.e.,  $\mathbf{P}_{(t,n)} = \mathbf{X}_{(t,s)} \mathbf{E}_{(s,n)}$ .

## 4 Results and discussion

### 4.1 Seasonal and interannual variability of UTLS temperature

First, we compared COSMIC profiles (both dry and wet profiles) with temperature, water vapor pressure, and refractivity profiles from 24 radiosonde stations across the GBM river basin from August 2006 to December 2013. The results (see Supplement) confirmed those of the previous studies (e.g., Sun et al., 2010; Kumar et al., 2011; Ansari et al., 2015) with radiosondes over India (referred to as IMD/MK4) and Bangladesh indicating substantial bias in the UTLS. The results from three recently upgraded radiosondes (over India) show significantly reduced bias in the UTLS with respect to the COSMIC RO data, suggesting that incorporating GPS receivers in conventional radiosondes helps to provide better estimates of temperature and water vapor profiles through more accurate measurement of pressure at various altitude levels (see Supplement). This highlights the importance of RO data in providing state-of-the-art data for calibrating existing radiosondes.

Figure 4 shows the regional mean temporal evolution of UTLS (dry) temperature anomalies (time mean removed). For COSMIC, dry temperature anomalies are plotted in Fig. 4a. The temperature anomalies range between ±6°C, indicating largest values above 50 hPa level (lower stratosphere) and below 200 hPa (troposphere). A strong seasonal cycle is evident in the troposphere below 200 hPa level and the stratosphere (above 70 hPa level). The three data sets (COSMIC, MERRA, and ERA-Interim) agree very well above 200 hPa where water vapor is negligible. Below

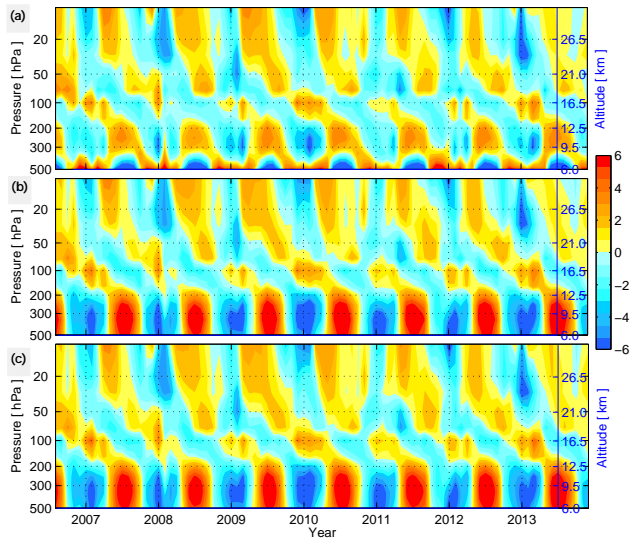


**Figure 4.** Temporal evolution of temperature (°C) with the time mean removed at each pressure level (500–10 hPa) based on (a) COSMIC RO, (b) MERRA, and (c) ERA-Interim. Data span between August 2006 and December 2013 and contain area-average over the region (16–35° N, 71–100° E) covering the GBM river basin.

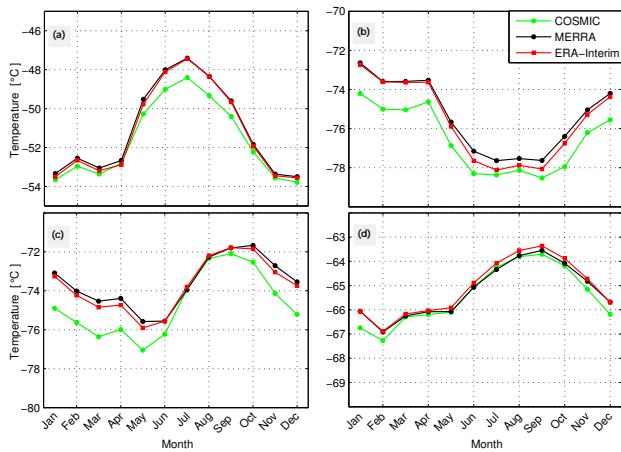


**Figure 5.** Seasonal cycle of temperature (°C) at (a) 200 hPa, (b) 100 hPa, (c) 70 hPa, and (d) 50 hPa from August 2006 to December 2013 based on COSMIC RO, MERRA, and ERA-Interim averaged over the GBM river basin.

200 hPa level, however, COSMIC data (Fig. 4a) are found to be colder than the two reanalyses (Fig. 4b–c) as the effect of water vapor becomes more significant. Both MERRA and ERA-Interim show quantitatively similar biases with respect to the COSMIC RO data, indicating a bias of 1.23 and 1.22 °C, respectively, when averaged over 200 to 70 hPa level, whereas the difference between MERRA and ERA-Interim was found to be  $\pm 0.5$  °C over the same layer during the last 89 months. The annual cycle of temperature at

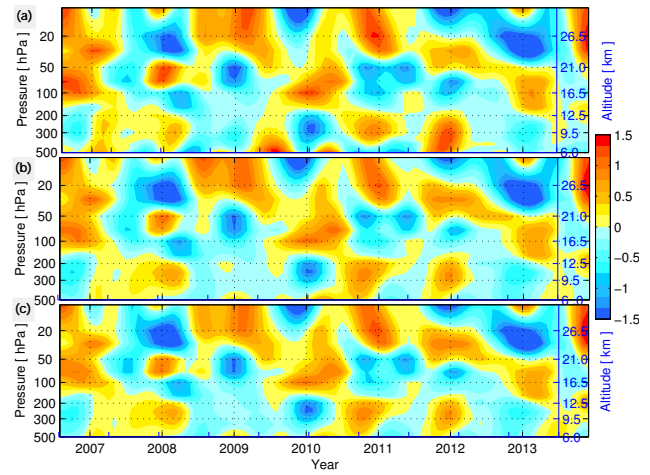


**Figure 6.** Interannual variability of temperature (°C) in the UTLS region based on (a) COSMIC RO, (b) MERRA, and (c) ERA-Interim from August 2006 to December 2013.

(a) 200 hPa, (b) 100 hPa, (c) 70 hPa, and (d) 50 hPa levels are shown in Fig. 5 to estimate the absolute bias (against COSMIC RO data) in reanalysis temperature data. Both MERRA and ERA-Interim indicate warm bias at all the levels with varying magnitudes over different seasons. Both reanalysis products are found to be warmer by  $\sim 1$  °C in June at 200 hPa level (Fig. 5a),  $\sim 1.5$  °C at 100 hPa level (Fig. 5b), and up to 2 °C at 70 hPa level from November to May (Fig. 5c).

Figure 6 shows the detrended (as well as deseasonalized) time series of temperature anomalies at four pressure levels mentioned above. The temperature anomalies show considerable interannual variability from 2006 to 2013, indicating large negative anomalies in the troposphere during 2009/2010 winter and early 2013, and the low stratosphere during 2007/2008, 2008/2009, and 2012/2013 winters. The 100 hPa level was warmer by  $\sim 1.5$  °C during the period 2006/2007, 2009/2010, and 2012/2013, and this is consistent in all the three data sets (Fig. 6a–c). The warm anomalies at the 100 hPa level for all three periods coincide with warm (i.e., El Niño) ENSO phase, while anomalously cold temperatures at 50 hPa level during 2009/2010 and 2010/2011 coincides with the recent stratospheric sudden warming (SSW) events. The stratospheric planetary waves in the winter Northern Hemisphere can become so intense that they can rapidly disrupt the northern polar vortex, replacing the westerly winds with easterly winds at high latitudes, leading to a dramatically warm polar stratosphere. This phenomenon is called SSW (Baldwin et al., 2001) and has a tendency to cool the stratosphere in the tropics and subtropics (e.g., 50 hPa level in Fig. 6). The temperature decreased by about 5 °C during the 2008/2009 SSW event at 50 hPa level (see also Resmi et al., 2013). The SSW events can occur during both westerly and easterly phase of the QBO, in which both 2008/2009 and 2010/2011 events occurred dur-

**Table 1.** Correlation coefficients between ocean–atmospheric climate indices and temperature anomalies at 200, 100, 70, and 50 hPa for the period August 2006 to December 2013. The values that are significant at 95 % confidence level based on the reduced degree of freedom are bolded.

Pressure levels	ENSO		IOD		QBO	
	Correlation	Lag (months)	Correlation	Lag (months)	Correlation	Lag (months)
200 hPa	<b>-0.70</b>	0	<b>-0.42</b>	0	0.39	26
100 hPa	<b>0.82</b>	1	0.27	2	<b>0.47</b>	27
70 hPa	<b>0.40</b>	3	-0.35	-4	<b>-0.45</b>	25
50 hPa	0.27	1	0.34	2	<b>0.53</b>	12

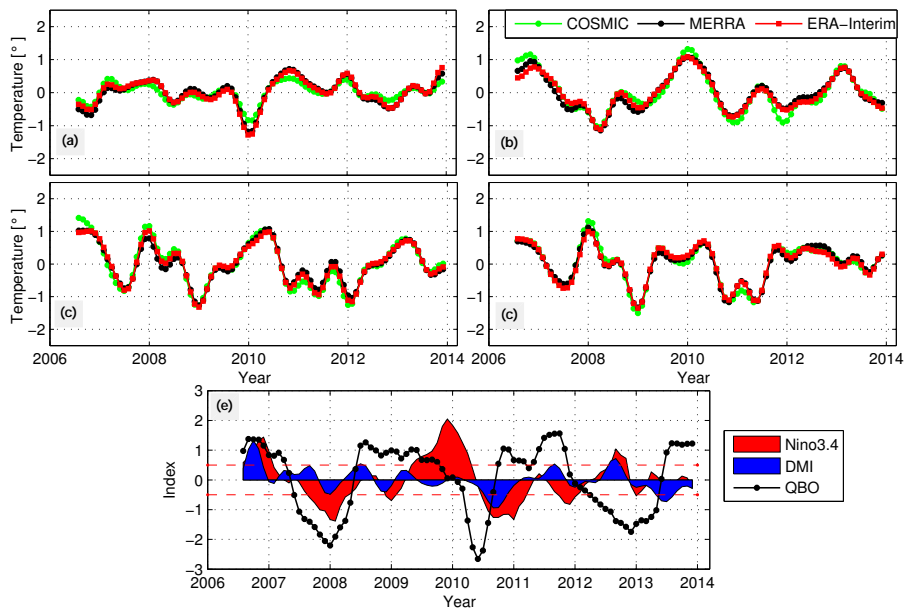


**Figure 7.** Interannual variability of temperature ( $^{\circ}\text{C}$ ) at (a) 200 hPa, (b) 100 hPa, (c) 70 hPa, and (d) 50 hPa from August 2006 to December 2013 based on COSMIC RO, MERRA, and ERA-Interim. (e) Ocean–atmospheric indices: Niño3.4, DMI, and QBO are also plotted for reference.

ing the westerly phase. The warm temperatures during 2006–2007 at the UTLS are associated with the combined impacts of ENSO and IOD, whereas positive temperature anomalies above 50 hPa possibly indicate a weak SSW.

In order to relate them to the three ocean–atmospheric indices described in Sect. 3.3, the temperature anomalies at (a) 200 hPa, (b) 100 hPa, (c) 70 hPa, and (d) 50 hPa are plotted in Fig. 7a–d together with the three indices in Fig. 7e. The 200 hPa level temperature anomalies clearly indicate the influence of 2009/2010 El Niño event (Fig. 7a) where temperature decreased by  $\sim 1.5^{\circ}\text{C}$  when El Niño was at its peak in January 2010 (Fig. 7a). The 200 hPa level temperatures are negatively correlated with ENSO (Fig. 7e) and 100 hPa level temperature (Fig. 7b). The 100 hPa level, whose temperatures are highly correlated with ENSO (see Table 1), also appears to be closely associated with the QBO anomalies especially during 2008/2009 and 2010/2011 (Fig. 7b). The

temperature anomalies at 70 and 50 hPa levels (Fig. 7c–d) primarily depict the structure of recent major SSW events (see also, Fig. 6), both of which occurred during the westerly phase of the QBO cycle. Correlation coefficients between temperature anomalies at these four pressure levels and three atmospheric/ocean indices are given in Table 1. Significance of the correlations is tested at 95 % confidence level using a reduced degree of freedom, which was obtained by dividing the total number of months ( $n = 89$ ) by 4 months that are used to smooth the time series.

As shown in Fig. 7, ENSO is highly correlated (0.82 at 1-month time lag) with temperatures at 100 hPa level and tend to be insignificant above 70 hPa level. Warmer (colder) SST leads to stronger (weaker) convection resulting in colder (warmer) tropopause temperatures and are also negatively correlated with temperatures at 200 hPa level. Both MERRA and ERA-Interim show similar correlation coefficients (re-

**Table 2.** Trends in temperature ( $^{\circ}\text{C year}^{-1}$ ) at 200, 100, 70, and 50 hPa for the period August 2006 to December 2013. Uncertainties in trend estimates are reported at 95 % confidence interval.

Pressure levels	COSMIC	MERRA	ERA-Interim
200 hPa	$0.02 \pm 0.02$	$0.03 \pm 0.03$	$0.03 \pm 0.05$
100 hPa	$-0.04 \pm 0.05$	$0.00 \pm 0.00$	$-0.02 \pm 0.04$
70 hPa	$-0.07 \pm 0.05$	$-0.04 \pm 0.05$	$-0.05 \pm 0.05$
50 hPa	$-0.02 \pm 0.04$	$-0.01 \pm 0.01$	$-0.01 \pm 0.02$

sults not shown). Since the IOD phenomenon is closely associated with the ENSO events between 2006 and 2013 (with a correlation coefficient of 0.42), it is found to be significantly correlated with temperatures in the lower troposphere with a correlation of  $-0.53$  at 400 hPa level (see Table 1). At the 200 hPa level, its correlation decreased to  $-0.42$  (see Table 1) but is still significant at 95 % confidence level. Temperatures at 100 hPa level over the tropics have been shown as an approximation of the QBO signal in Liang et al. (2011) due their very high correlation (0.86) between 2004 and 2010. However, their relationship did not hold steady (with a correlation of 0.47 at 100 hPa level) as the QBO westerly phase slowed dramatically lasting for about 21 months (i.e., 1 and 1/2 cycle) from June 2008 to January 2010, followed by a step easterly phase in June 2010.

Temperature changes estimated at the four pressure levels (Fig. 6) from 2006 to 2013 are given in Table 2. The linear trends are estimated from the deseasonalized temperature anomalies using non-parametric Sen’s slope estimator (Sen, 1968). Significance of trends are tested at 95 % confidence level based on the Mann–Kendall non-parametric test (Mann, 1945; Kendall, 1962). Consistent with the time series shown in Fig. 6a, there is a slight increase (but not significant) in temperature ( $0.02 \pm 0.02 \text{ }^{\circ}\text{C year}^{-1}$  based on COSMIC RO) at 200 hPa level and a decrease in temperature ( $-0.04 \pm 0.05 \text{ }^{\circ}\text{C year}^{-1}$  based on COSMIC RO) at the 100 hPa level. It also confirms the recent stratospheric cooling trends (Seidel et al., 2011), indicating a temperature decrease at the rate of  $0.07 \pm 0.05 \text{ }^{\circ}\text{C year}^{-1}$  based on COSMIC RO at 70 hPa level during the past 8 years. These trends are also consistently estimated by the two reanalysis products (MERRA and ERA-Interim) except at 100 hPa level where MERRA data did not show any trend (see Table 2). The uncertainties in trend estimates were relatively larger than the trend themselves due to the short time span but nevertheless the trends are clearly visible at different levels (see Fig. 7).

#### 4.2 Trends and variability of tropopause heights and temperatures

The annual mean and standard deviation of tropopause temperatures and heights are plotted in Figs. 8 and 9. The tropopause is generally colder (higher) in south (closer to the equator), reaching a minimum (maximum) tempera-

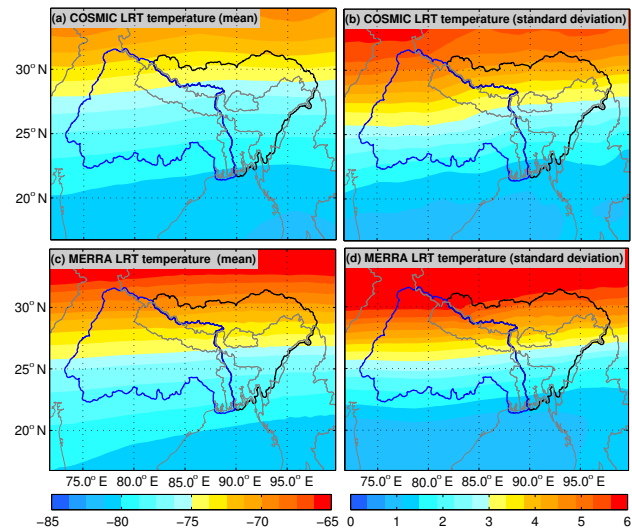


**Figure 8.** Spatial variation of mean and standard deviation of tropopause temperatures ( $^{\circ}\text{C}$ ) derived from COSMIC RO and MERRA product based on 89 months from August 2006 to December 2013. (a) Mean and (b) standard deviation of tropopause temperatures ( $^{\circ}\text{C}$ ) from COSMIC RO; (c) mean and (d) standard deviation of tropopause temperatures ( $^{\circ}\text{C}$ ) from MERRA product.

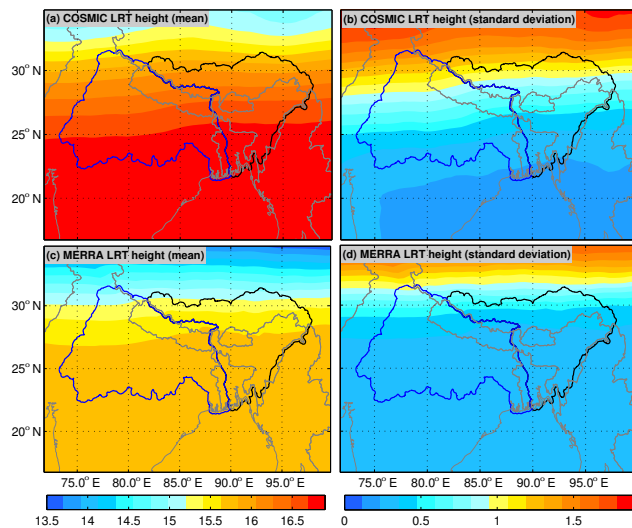


**Figure 9.** Spatial variation of mean and standard deviation of tropopause heights (km) derived from COSMIC RO and MERRA product based on 89 months from August 2006 to December 2013. (a) Mean and (b) standard deviation of tropopause heights (km) from COSMIC RO; (c) mean and (d) standard deviation of tropopause heights (km) from MERRA product.

ture (height) of  $-81.5 \text{ }^{\circ}\text{C}$  (16.9 km) over southern Myanmar (Figs. 8a and 9a). While the temperature gradually increases from south to north (from  $-81.5$  to  $-69.5 \text{ }^{\circ}\text{C}$ , based on COSMIC RO in Fig. 8a), its heights are more or less homogenous at around 16.8 km below  $29^{\circ}\text{N}$  with its boundary roughly falling on the northern boundaries of Bhutan. However, its

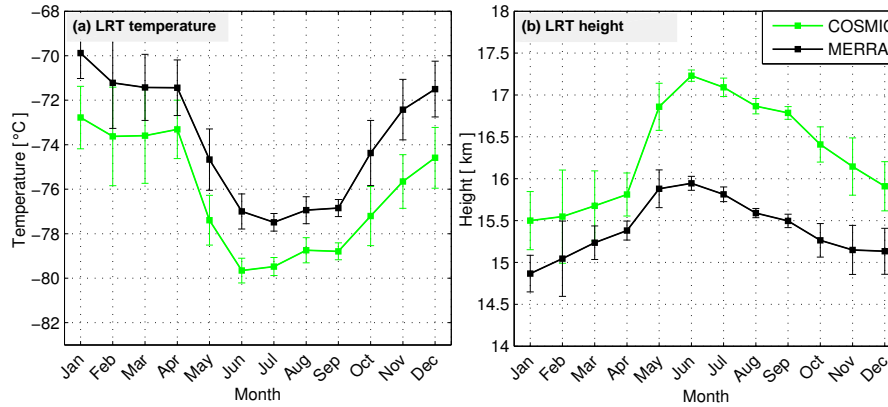


**Figure 10.** Annual cycle of tropopause over the GBM river basin computed from MERRA and COSMIC RO data for the period between August 2006 and December 2013: (a) tropopause temperatures and (b) tropopause heights.

height changes steeply by around 2 km from 29 to 35° N, which also shows the largest standard deviation ( $\sim 1.8$  km, Fig. 9b). The standard deviations of temperatures reaches up to  $\pm 6$  °C based on COSMIC RO data (Fig. 8b) over the same region.

The tropopause over the GBM river basin often reaches as high as 18 km in response to the Indian summer monsoon, when intense convective activities occur, and as low as 10 km during winter. The spatial patterns of tropopause shown by MERRA are consistent with those from COSMIC RO but are found to be more zonally homogenous, warmer (by up to 4 °C in the north) and lower (by  $\sim 1$  km) over the region. This warm bias (against COSMIC RO data) is also observed in ERA-Interim at 100 hPa level (see Fig. 5b) but is relatively lower than MERRA, especially during the monsoon. The annual cycle of area-averaged (over the spatial domain covering 71.5–99.5° E, 16.5–34.5° N) tropopause temperatures and heights of COSMIC RO and MERRA are shown in Fig. 10. The area-averaged temperatures (heights) of COSMIC RO reach minimum (maximum) in June but are warmer (lower) in MERRA by 1.0–2.5 °C ( $\sim 1.2$  km from May to December). MERRA also shows the tropopause temperature minimum in July instead of June (Fig. 10a). The large differences in MERRA could partly be related to the approximation in Eq. (1), but it should be noted that errors in tropopause heights may cause large errors in temperature due to the lapse-rate criterion. The warm bias (against COSMIC RO data) observed in reanalysis products was thought to mainly stem from assimilation of radiance observations from aircrafts and satellites (see, e.g., Dee et al., 2011, and references therein). Large variations in tropopause temperatures and heights in Fig. 10 (indicated by error bars) during winter and spring could be related to high diurnal temperature variations (Mehta et al., 2010).

The annual cycle was removed from each grid cell to examine the interannual variability of tropopause temperatures and heights and to estimate linear trends over the period Au-

**Table 3.** Trends in tropopause temperatures ( $^{\circ}\text{C year}^{-1}$ ) and heights ( $\text{m year}^{-1}$ ) based on the area-averaged time series anomalies derived from COSMIC RO and MERRA. Data span between August 2006 and December 2013. Uncertainties in trend estimates are reported at 95 % confidence interval.

Data	Temperature ( $^{\circ}\text{C year}^{-1}$ )	Height ( $\text{m year}^{-1}$ )
COSMIC RO	$-0.039 \pm 0.05$	$6.01 \pm 5.02$
MERRA	$-0.005 \pm 0.03$	$17.00 \pm 10.20$

gust 2006 to December 2013. The area-averaged linear trends and their uncertainties are given in Table 3. In general, based on the COSMIC RO data, the tropopause appears to be cooling (increasing in height) at a rate of  $-0.039 \pm 0.05$  °C year $^{-1}$  ( $6.01 \pm 5.02$  m year $^{-1}$ ) during the period (see Table 3), which to some degree is also estimated by MERRA. However, MERRA shows negligible cooling compared to COSMIC RO while its height increase is not consistent with its temperature decline. The increasing (decreasing) tropopause heights (temperatures) has been consistently observed in GNSS RO data over the years at both global and regional scale (e.g., Schmidt et al., 2008, 2010; Khandu et al., 2011), which is evidently in response to enhanced warming in the upper troposphere and substantial cooling in the lower stratosphere.

Next, PCA is applied on the deseasonalized time series of tropopause temperatures and heights in order to study the spatio-temporal characteristics of tropopause over the GBM river basin. PCA is particularly relevant here because tropopause is a transitional layer that responds to perturbations from both the troposphere and stratosphere, which makes it difficult to understand their variability modes. Figure 11 shows the EOFs (or spatial maps) of the first three leading modes of variability. The first EOF accounts for a variability of  $\sim 73$  % (COSMIC RO) and  $\sim 63$  % (MERRA) indicating positive anomalies (up to 1.1 °C) across the GBM river basin. EOF 1 appears to be rather symmetric around

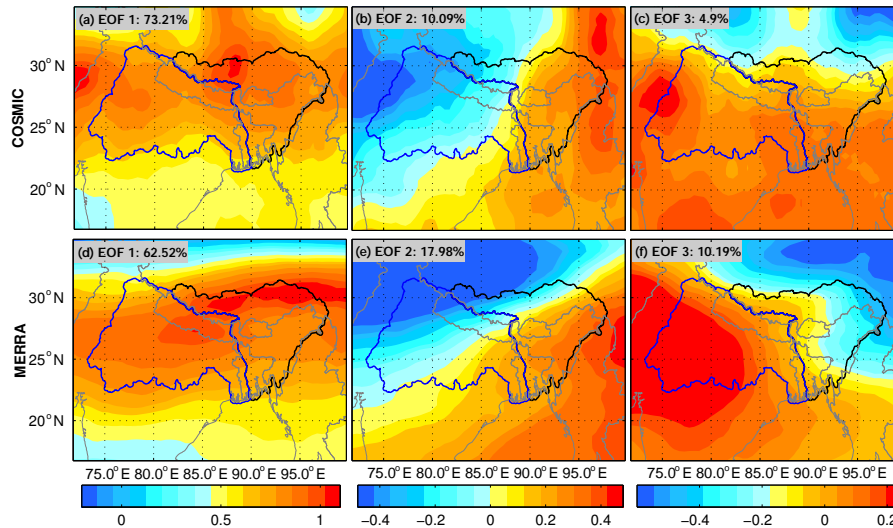


**Figure 11.** The first three leading EOFs of tropopause temperature ( $^{\circ}\text{C}$ ) based on MERRA data and COSMIC RO data for the period August 2006 to December 2013.

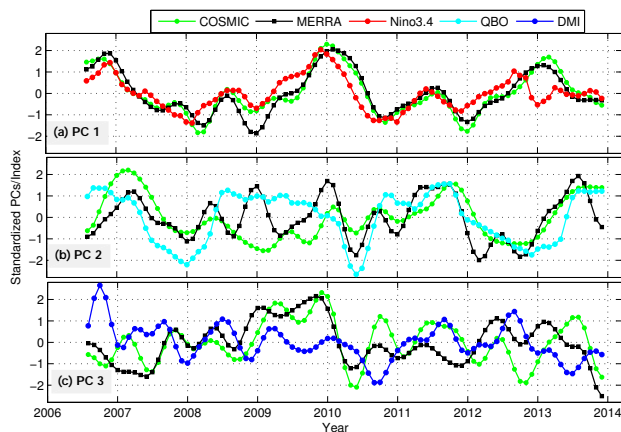


**Figure 12.** The corresponding PCs (temporal components) based on the three leading orthogonal modes shown in Fig. 11.

$29^{\circ}\text{N}$  in COSMIC RO but seems to be shifted slightly southwards in MERRA (Fig. 11a and d). Their corresponding PCs are shown in Fig. 12. PC 1 (Fig. 12a) is found to be highly correlated with Niño3.4 index with a correlation of 0.77 (COSMIC RO) and 0.78 (MERRA) with a time lag of 1 month, indicating that ENSO dominates tropopause variability over the region (see Table 4). DMI is also moderately correlated (0.35) with PC 1 of both COSMIC RO and MERRA (with a lag of 2 months), indicating that warmer SSTs in the equatorial Indian ocean might be having some influence on the tropopause variability.

The second EOF shown in Fig. 11b and e indicates a diagonal (dipole) pattern with positive (negative) anomalies in the northwest (southeast), accounting for variance of  $\sim 10\%$  (COSMIC) and  $\sim 18\%$  (MERRA). Its corresponding PC

is found to be significantly correlated with the QBO index with a correlation coefficient of 0.40 (COSMIC RO) and 0.53 (MERRA) (at zero lag). It is not surprising that the relationship between PC 2 and QBO is relatively low compared to the equatorial (or tropical) tropopause since QBO is a tropical phenomenon (e.g., Reid and Gage, 1985; Randel et al., 2000; Gettelman et al., 2001; Liang et al., 2011). It also stems from the fact that QBO westerly phase prolonged for an extended period of 21 months before changing to a westerly phase in January 2010. The third EOF (Fig. 11c and f) explains about 5% (COSMIC RO) and 10% (MERRA) of the variability and shows positive (negative) anomalies below (above)  $30^{\circ}\text{N}$ , although MERRA shows a diagonal dipole pattern similar to EOF 2. Their corresponding PCs are found to be moderately correlated with ENSO and IOD. The tropopause heights are negatively correlated with their temperatures and, therefore, vary inversely with its temperature, i.e., increase in tropopause height with decrease in temperature (figures not shown). The correlation coefficient between the PCs of three leading modes of tropopause heights and the ocean–atmospheric indices indicate similar magnitudes of correlations but with opposite signs (see Table 4).

To show the influence of ENSO mode on the tropopause, the seasonal mean area-averaged anomalies of tropopause temperatures and heights are plotted in Fig. 13. Seasonal mean anomalies are obtained by averaging the products of EOF 1 and PC 1 (of the COSMIC RO data). The ENSO effect is found to be maximum during the winter (e.g., 2009–2010, 2012–2013) when ENSO was at its peak. Its effects are also felt during autumn (in 2007 and 2011) and spring (in 2008) and during the El Niño and La Niña periods. The largest tropopause anomaly occurred during the major

**Table 4.** Correlation coefficients between tropopause parameters (temperature and height) derived from COSMIC RO and MERRA and ocean–atmospheric indices for the period August 2006 to December 2013. The values that are significant at 95 % confidence level based on the reduced degree of freedom are bolded.

Data	COSMIC RO		MERRA	
	Temperature	Height	Temperature	Height
Nino3.4 & PC 1	<b>0.77</b>	<b>−0.74</b>	<b>0.78</b>	<b>−0.75</b>
IOD & PC 1	0.35	0.37	0.35	0.38
QBO & PC 2	0.36	0.36	<b>0.53</b>	<b>0.54</b>

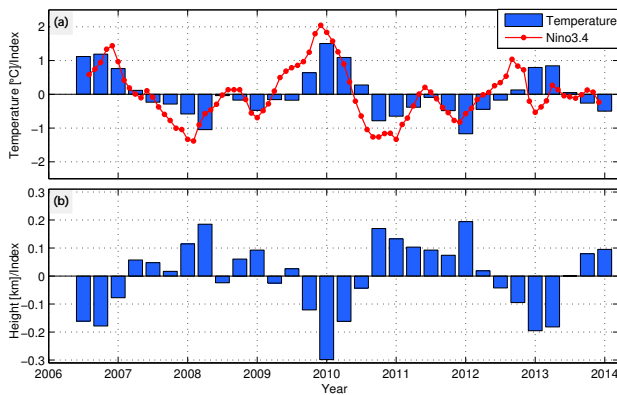


**Figure 13.** Seasonal mean tropopause temperature and height anomalies due to ENSO mode together with the Niño3.4 index. The area-averaged time series were obtained by multiplying EOF 1 and PC 1, i.e., basically showed the replication of ENSO mode.

El Niño event of 2009/2010 when tropopause temperature (height) increased (decreased) by about 1.5 °C (300 m) in the winter (Fig. 13a–b). La Niña periods (e.g., 2007/2008, 2010/2011) are mainly associated with deep convections in the troposphere leading to a wider troposphere or higher tropopause height (see Fig. 13b).

## 5 Conclusions

This study examines the interannual variability of temperature in the UTLS including tropopause temperatures and heights over the GBM river basin in South Asia using 89 months (August 2006 to December 2013) of COSMIC RO data and two global reanalyses (MERRA and ERA-Interim). The GBM river basin received an average of  $\sim 576$  well-distributed COSMIC RO profiles/month during the period with more than 56 % of the profiles reaching at least 1.5 km above the mean sea level height. Even though the reanalysis products such as MERRA and ERA-Interim are significantly warmer (by up to 2 °C) than COSMIC RO data at 200–50 hPa level, the warm bias is found to be consistent over time. The UTLS temperature showed considerable interannual variability during the past 8 years (2006–2013) with modest trends in

the troposphere and stratosphere. ENSO is found to have the largest effect at the 100 hPa level with a correlation of 0.82 (at 1-month lag) while SSW signals tend to dominate the lower stratospheric temperature anomalies (e.g., at 50 hPa level). The temperature at 200 hPa level decreased by  $\sim 1.5$  °C during the last major El Niño event of 2009/2010. The SSW events that occurred in 2008/2009 and 2010/2011 winters are marked by pronounced cooling at 50 hPa level.

The relationship between ENSO and QBO has been reported to be strong between 2004 and 2008 (see Liang et al., 2011) but has weakened substantially over the years due to a persistent westerly phase that lasted for 21 months from June 2008 to January 2010. The IOD mode plays a significant role on the tropospheric temperature warming over the GBM river basin as enhanced upwellings in the equatorial Indian ocean drives more convection in the region. However, their role seems to be limited within the troposphere as the magnitude of correlation between DMI and temperature decreases from  $-0.53$  at 400 hPa level to  $-0.42$  hPa at 200 hPa level. Consistent with the previous studies, there is a warming (cooling) trend in the upper troposphere (lower stratosphere), which is consistent with other estimated global warming trends (see, e.g., IPCC, 2007, 2013, and references therein).

The tropopause temperatures and heights derived from COSMIC RO and MERRA were investigated in detail due to their importance in climate change and attribution studies (see, e.g., Santer et al., 2003a, 2008; IPCC, 2007). The interannual variability of tropopause temperatures and heights over the GBM river basin was studied by applying the PCA method. The results indicate a dominant effect of ENSO, accounting for a variance of about 73 % (COSMIC RO) and 63 % (MERRA) of the first variability mode. PC 1 shows a near-accurate representation of the ENSO mode (represented by the Niño3.4 index) with a correlation of 0.77 (COSMIC RO) and 0.78 (MERRA). The QBO accounts for  $\sim 10$  % (COSMIC RO) and  $\sim 18$  % (MERRA) of the variability, as indicated by the correlation between PC 2 and the QBO index. The largest temperature anomaly was recorded in 2009/2010 winter corresponding to a major El Niño event. The tropopause temperatures (heights) increased (decreased in heights) by about 1.5 °C (300 m) during this period. Because IOD effects are generally found to be concentrated within the troposphere, the correlations between and DMI and tropopause (temperature and height) are found to be low but, nevertheless, require further examination using longer time series.

**Acknowledgements.** The authors are very grateful to the Associate Editor, Gabriele Stiller, and the two anonymous reviewers for their comments, which helped to significantly improve the quality of this manuscript. Khandu is grateful to Curtin Strategic International Research Scholarship, Curtin University (Australia), for the financial support. He also acknowledges the financial support of Prince Albert II of Monaco Foundation and the Intergovernmental Panel on Climate Change (IPCC). Joseph Awange appreciates the financial support from both Alexander von Humboldt and Japan Society of Promotion of Science for his stay at Karlsruhe Institute of Technology (Germany) and Kyoto University (Japan), respectively. Ehsan Foroootan is grateful for the research grant from the German Aerospace Center (DLR). The authors are very grateful to the University Corporation for Atmospheric Research (UCAR) community for providing both COSMIC RO profiles and radiosonde data sets used in this study. The authors are also thankful to National Aeronautics and Space Administration (NASA) and European Center for Medium range Weather Forecasting (ECMWF) for providing reanalysis products that were used to complete this study (D-SAT project Fkz.: 50 LZ 1402).

Edited by: G. Stiller

## References

- Ansari, M. I., Madan, R., and Bhaita, S.: Verification of quality of GPS based radiosonde data, *Mausam*, 66, 367–374, available at: [metnet.imd.gov.in/mausamdocs/16632\\_F.pdf](http://metnet.imd.gov.in/mausamdocs/16632_F.pdf), 2015.
- Anthes, R. A.: Exploring Earth's atmosphere with radio occultation: contributions to weather, climate and space weather, *Atmos. Meas. Tech.*, 4, 1077–1103, doi:10.5194/amt-4-1077-2011, 2011.
- Anthes, R. A., Ector, D., Hunt, D. C., Kuo, Y. H., Rocken, C., Schreiner, W. S., Sokolovskiy, S. V., Syndergaard, S., Wee, T. K., Zeng, Z., Bernhardt, P. A., Dymond, K. F., Chen, Y., Liu, H., Manning, K., Randel, W. J., Trenberth, K. E., Cucurull, L., Healy, S. B., Ho, S. P., McCormick, C., Meehan, T. K., Thompson, D. C., and Yen, N. L.: The COSMIC/FORMOSAT-3 mission: early results, *B. Am. Meteorol. Soc.*, 89, 313–333, doi:10.1175/BAMS-89-3-313, 2008.
- Ashok, K. and Saji, N. H.: On the impacts of ENSO and Indian Ocean dipole events on sub-regional Indian summer monsoon rainfall, *Nat. Hazards*, 42, 273–285, doi:10.1007/s11069-006-9091-0, 2007.
- Baldwin, M. P., Gray, L. J., Dunkerton, T. J., Hamilton, K., Haynes, P. H., Randel, W. J., Holton, J. R., Alexander, M. J., Hirota, I., Horinouchi, T., Jones, D. B. A., Kinnerson, J. S., Marquardt, C., Sato, K., and Takahashi, M.: The quasi-biennial oscillation, *Rev. Geophys.*, 39, 179–229, doi:10.1029/1999RG000073, 2001.
- Chowdhury, M. R.: The El Niño-Southern Oscillation (ENSO) and seasonal flooding – Bangladesh, *Theor. Appl. Climatol.*, 76, 105–124, doi:10.1007/s00704-003-0001-z, 2003.
- Chowdhury, M. D. R. and Ward, N.: Hydro-meteorological variability in the greater Ganges–Brahmaputra–Meghna basins, *Int. J. Climatol.*, 24, 1495–1508, doi:10.1002/joc.1076, 2004.
- Cucurull, L., Derber, J. C., Treadon, R., and Purser, R.: Assimilation of Global Positioning System radio occultation observations into NCEP's Global Data Assimilation System, *Mon. Weather Rev.*, 35, 3174–3193, doi:10.1175/MWR3461.1, 2007.
- Das Gupta, M., Das, S., Prasanthi, K., and Pradhan, P. K.: Validation of upper-air observations taken during the ARMEX-I and its impact on the global analysis-forecast system, *Mausam*, 56, 139–146, 2005.
- Dee, D. P., Uppala, S. M., Simmons, A. J., Berrisford, P., Poli, P., Kobayashi, S., Andrae, U., Balmaseda, M. A., Balsamo, G., Bauer, P., Bechtold, P., Beljaars, A. C. M., van de Berg, L., Bidlot, J., Bormann, N., Delsol, C., Dragani, R., Fuentes, M., Geer, A. J., Haimberger, L., Healy, S. B., Hersbach, H., Holm, E. V., Isaksen, I., Kållberg, P., Köhler, M., Matricardi, M., McNally, A. P., Monge-Sanz, B. M., Morcrette, J.-J., Park, B.-K., Peubey, C., de Rosnay, P., Tavolato, C., Thépaut, J.-N., and Vitarta, F.: The ERA-Interim reanalysis: configuration and performance of the data assimilation system, *Q. J. Roy. Meteor. Soc.*, 137, 553–597, doi:10.1002/qj.828, 2011.
- Foelsche, U., Borsche, M., Steiner, A. K., Gobiet, A., Pirscher, B., Kirchengast, G., Wickert, J., and Schmidt, T.: Observing upper troposphere–lower stratosphere climate with radio occultation data from the CHAMP satellite, *Clim. Dynam.*, 31, 49–65, doi:10.1007/s00382-007-0337-7, 2008.
- Gautam, R., Hsu, N. C., Lau, K. M., Tsay, S. C., and Kafatos, M.: Enhanced Pre-Monsoon Warming over the Himalayan-Gangetic Region from 1979 to 2007, *Geophys. Res. Lett.*, 36, L07704, doi:10.1029/2009GL037641, 2009.
- Gettelman, A., Randel, W. J., Massie, S., Wu, F., Read, W. G., and Russell, J. M.: El Niño as a Natural Experiment for Studying the Tropical Tropopause Region, *J. Climate*, 14, 3375–3392, doi:10.1175/1520-0442(2001)014<3375:ENOAAN>2.0.CO;2, 2001.
- Goovaerts, P.: Geostatistical approaches for incorporating elevation into the spatial interpolation of rainfall, *J. Hydrol.*, 228, 113–129, doi:10.1016/S0022-1694(00)00144-X, 2000.
- Healy, S. B. and Thépaut, J.-N.: Assimilation experiments with CHAMP GPS radio occultation measurements, *Q. J. Roy. Meteor. Soc.*, 132, 605–623, doi:10.1256/qj.04.182, 2006.
- Ho, S. P., Zhou, X., Kuo, Y. K., Hunt, D., and Wang, J. H.: Global Evaluation of Radiosonde Water Vapor Systematic Biases using GPS Radio Occultation from COSMIC and ECMWF Analysis, *Remote Sens.*, 2, 1320–1330, doi:10.3390/rs2051320, 2010.
- IPCC: Summary for Policymakers, in: *Climate Change 2007: The Physical Science Basis, Contribution of Working Group I to the Fifth Assessment Report of the Intergovernmental Panel on Climate Change*, edited by: Solomon, S., Qin, D., Manning, M., Chen, Z., Marquis, M., Averyt, K., Tignor, M., and Miller, H., Cambridge University Press, Cambridge, United Kingdom and New York, USA, 2007.
- IPCC: Summary for Policymakers, in: *Climate Change 2013: The Physical Science Basis, Contribution of Working Group I to the Fifth Assessment Report of the Intergovernmental Panel on Climate Change*, edited by: Stocker, T. F., Qin, D., Plattner, G. K., Tignor, M., Allen, S. K., Boschung, J., Nauels, A., Xia, Y., Bex, V., and Midgley, P., Cambridge University Press, Cambridge, United Kingdom and New York, USA, 2013.
- Karl, T. R., Hassol, S. J., Miller, C. D., and Murray, W. L. (Eds.): *Temperature Trends in the Lower Atmosphere: Steps for Understanding and Reconciling Differences*, Tech. rep., US Climate Change Science Program, Washington, DC, 2006.

- Kendall, M. G.: Rank correlation methods, *J. Am. Stat. Assoc.*, 63, 1379–1389, doi:10.1080/01621459.1968.10480934, 1962.
- Khandu, Awange, J. L., Wickert, J., Schmidt, T., Sharifi, M. A., Heck, B., and Fleming, K.: GNSS remote sensing of the Australian tropopause, *Climate Change*, 105, 597–618, doi:10.1007/s10584-010-9894-6, 2011.
- Kumar, G., Madan, R., Saikrishnan, K., Kundu, S. K., and Jain, P. K.: Technical and operational characteristics of GPS sounding system in the upper air network of IMD, *Mausam*, 62, 403–416, available at: [metnet.imd.gov.in/mausamdocs/16632\\_F.pdf](http://metnet.imd.gov.in/mausamdocs/16632_F.pdf), 2011.
- Kunze, M., Braesicke, P., Langematz, U., Stiller, G., Bekki, S., Brühl, C., Chipperfield, M., Dameris, M., Garcia, R., and Giorgetta, M.: Influences of the Indian Summer Monsoon on Water Vapor and Ozone Concentrations in the UTLS as Simulated by Chemistry-Climate Models, *J. Climate*, 23, 3525–3544, doi:10.1175/2010JCLI3280.1, 2010.
- Lau, W. K. M., Kim, K. M., Hsu, C. N., and Holben, B. N.: Possible influences of air pollution, dust- and sandstorms on the Indian monsoon, *Bulletin – World Meteorological Organization*, 58, 22–30, 2009.
- Lee, I. T., Matsuo, T., Richmon, A. D., Liu, J. Y., Wang, W., Lin, C. H., Anderson, J. L., and Chen, M. Q.: Assimilation of FORMOSAT-3/COSMIC electron density profiles into a coupled thermosphere/ionosphere model using ensemble Kalman filtering, *J. Geophys. Res.*, 117, A10318, doi:10.1029/2012JA017700, 2012.
- Liang, C. K., Eldering, A., Gettelman, A., Tian, B., Wong, S., Fetzer, E. J., and Liou, K. N.: Record of tropical interannual variability of temperature and water vapor from a combined AIRS-MLS data set, *J. Geophys. Res.*, 116, D06103, doi:10.1029/2010JD014841, 2011.
- Lott, F. C., Stott, P. A., Mitchell, D. M., Christidis, N., Gillett, N. P., Haimberger, L., Perlwitz, J., and Thorne, P. W.: Models versus radiosondes in the free atmosphere: a new detection and attribution analysis of temperature, *J. Geophys. Res.*, 118, 2609–2619, doi:10.1002/jgrd.50255, 2013.
- Mann, H. B.: Nonparametric Tests Against Trend, *Econometrica*, 13, 245–259, 1945.
- Mehta, S. K., Ratnam, M. V., and Murthy, B. V. K.: Variability of the tropical tropopause over Indian monsoon region, *J. Geophys. Res.*, 115, D14120, doi:10.1029/2009JD012655, 2010.
- Melbourne, W. G., Davis, E. S., Duncan, C. B., Hajj, G. A., Hardy, K. R., Kursinski, E. R., Meehan, T. K., Young, L. E., and Yunck, T. P.: The application of spaceborne GPS to atmospheric limb sounding and global change monitoring, *Tech. Rep. JPL-PUBL-94-18*, Jet Propulsion Laboratory, California Institute of Technology, Pasadena, CA, US, 1994.
- Mirza, M. M. Q., Warrick, R., Ericksen, N., and Kenny, G.: Trends and persistence in precipitation in the Ganges, Brahmaputra and Meghna river basins, *Hydrological Sciences*, 43, 845–858, doi:10.1080/02626669809492182, 1998.
- Pan, L. L., Randel, W. J., Gary, B. L., Mahoney, M. J., and Hints, E. J.: Definitions and sharpness of the extratropical tropopause: A trace gas perspective, *Rev. Geophys.*, 109, D23103, doi:10.1029/2004JD004982, 2004.
- Poli, P., Healy, S. B., Rabier, F., and Pailleux, J.: Preliminary assessment of the scalability of GPS radio occultations impact in numerical weather prediction, *Geophys. Res. Lett.*, 35, L23811, doi:10.1029/2008GL035873, 2008.
- Poli, P., Healy, S. B., and Dee, D. P.: Assimilation of Global Positioning System radio occultation data in the ECMWF ERA–Interim reanalysis, *Q. J. Roy. Meteor. Soc.*, 136, 1972–1990, doi:10.1002/qj.722, 2010.
- Preisendorfer, R. W.: *Principal component analysis in meteorology and oceanography*, Elsevier, 1988.
- PSAS: A quick derivation relating altitude to air pressure, Portland State Aerospace Society, US, available at: [http://psas.pdx.edu/RocketScience/PressureAltitude\\_Derived.pdf](http://psas.pdx.edu/RocketScience/PressureAltitude_Derived.pdf), 2004.
- Randel, W. J., Wu, F., and Gaffen, D. J.: Interannual variability of the tropical tropopause derived from radiosonde data and NCEP reanalyses, *J. Geophys. Res.*, 105, 15509–15523, doi:10.1029/2000JD900155, 2000.
- Rao, V. B., Ferreira, C. C., Franchito, S. H., and Ramakrishna, S. S. V. S.: In a changing climate weakening tropical easterly jet induces more violent tropical storms over the north Indian Ocean, *Geophys. Res. Lett.*, 35, L15710, doi:10.1029/2008GL034729, 2008.
- Reid, G. C. and Gage, K. S.: Interannual variations in the height of the tropical tropopause, *J. Geophys. Res.*, 90, 5629–5635, doi:10.1029/JD090iD03p05629, 1985.
- Resmi, E., Mohanakumar, K., and Appu, K.: Effect of polar sudden stratospheric warming on the tropical stratosphere and troposphere and its surface signatures over the Indian region, *B. Am. Meteorol. Soc.*, 105–106, 15–29, doi:10.1016/j.jastp.2013.07.003, 2013.
- Rienecker, M. M., Suarez, M. J., Todling, R., Bacmeister, J., Takacs, L., Liu, H. C., Gu, W., Sienkiewicz, M., Koster, R. D., Gelaro, R., Stajner, I., and Nielsen, J. E.: The GEOS-5 Data Assimilation System Documentation of Versions 5.0.1, 5.1.0, and 5.2.0, NASA Technical Report Series on Global Modeling and Data Assimilation Vol. 27, NASA/TM–2008–104606, NASA Center for AeroSpace Information, Greenbelt, Maryland, US, 2008.
- Rienecker, M. M., Suarez, M. J., Gelaro, R., Todling, R., Bacmeister, J., Liu, E., Bosilovich, M. G., Schubert, S. D., Takacs, L., Kim, G. K., Bloom, S., Chen, J., Collins, D., Conaty, A., da Silva, A., Gu, W., Joiner, J., Koster, R. D., Lucchesi, R., Molod, A., Owens, T., Pawson, S., Pegion, P., Redder, C. R., Reichle, R., Robertson, F. R., Ruddick, A. G., Sienkiewicz, M., and Woollen, J.: MERRA: NASA’s Modern-Era Retrospective Analysis for Research and Applications, *J. Climate*, 24, 3624–3648, doi:10.1175/JCLI-D-11-00015.1, 2011.
- Rocken, C., Anthes, R., Exner, M., Hunt, D., Sokolovskiy, S., Ware, R., Gorbunov, M., Schreiner, W., Feng, D., Herman, B., Kuo, Y.-H., and Zou, X.: Analysis and validation of GPS/MET data in the neutral atmosphere, *J. Geophys. Res.*, 102, 29849–29866, doi:10.1029/97JD02400, 1997.
- Santer, B. D., Wehner, M. F., Wigley, T. M. L., R., Meehl, G. A., Taylor, K. E., Ammann, C., Arblaster, J., Washington, W. M., Boyle, J. S., and Brüggemann, W.: Contributions of anthropogenic and natural forcing to recent tropopause height changes, *Science*, 301, 479–483, doi:10.1126/science.1084123, 2003a.
- Santer, B. D., Sausen, Wigley, T. M. L., Boyle, J. S., and Doutriaux, K. A., Hansen, J. E., Meehl, G. A., Roeckner, E., Ruedy, R., Schmidt, G., and Taylor, K. E.: Behavior of tropopause height and atmospheric temperature in models, reanalyses, and observations: Decadal changes, *J. Geophys. Res.*, 108, ACL 1-1–ACL 1-22, doi:10.1029/2002JD00225, 2003b.

- Santer, B. D., Thorne, P. W., Haimberger, L., Taylor, K. E., Wigley, T. M. L., Lanzante, J. R., Solomon, S., Free, M., Gleckler, P. J., Jones, P. D., Karl, T. R., Klein, S. A., Mears, C., Nychka, D., Schmidt, G. A., Sherwood, S. C., and Wentz, F. J.: Consistency of modelled and observed temperature trends in the tropical troposphere, *Int. J. Climatol.*, 13, 1703–1722, doi:10.1002/joc.1756, 2008.
- Sausen, R. and Santer, B. D.: Use of changes in tropopause height to detect human influences on climate, *Meteorol. Z.*, 3, 131–136, doi:10.1127/0941-2948/2003/0012-0131, 2003.
- Schmidt, T., Wickert, J., Beyerle, G., and Heise, S.: Global tropopause height trends estimated from GPS radio occultation data, *Geophys. Res. Lett.*, 35, L11806, doi:10.1029/2008GL034012, 2008.
- Schmidt, T., Wickert, J., and Haser, A.: Variability of the upper troposphere and lower stratosphere observed with GPS radio occultation bending angles and temperatures, *Adv. Space Res.*, 46, 150–161, doi:10.1016/j.asr.2010.01.021, 2010.
- Seidel, D. J., Gillett, N. P., Lanzante, J. R., Shine, K. P., and Thorne, P. W.: Stratospheric temperature trends: our evolving understanding, *WIREs Climate Change*, 2, 592–616, doi:10.1002/wcc.125, 2011.
- Sen, P. K.: Estimates of the Regression Coefficient Based on Kendall's Tau, *J. Am. Stat. Assoc.*, 63, 1379–1389, doi:10.1080/01621459.1968.10480934, 1968.
- Steiner, A. K., Hunt, D., Ho, S.-P., Kirchengast, G., Mannucci, A. J., Scherllin-Pirscher, B., Gleisner, H., von Engel, A., Schmidt, T., Ao, C., Leroy, S. S., Kursinski, E. R., Foelsche, U., Gorbunov, M., Heise, S., Kuo, Y.-H., Lauritsen, K. B., Marquardt, C., Rocken, C., Schreiner, W., Sokolovskiy, S., Syndergaard, S., and Wickert, J.: Quantification of structural uncertainty in climate data records from GPS radio occultation, *Atmos. Chem. Phys.*, 13, 1469–1484, doi:10.5194/acp-13-1469-2013, 2013.
- Sun, B., Reale, A. J. D., and Hunt, D. C.: Comparing radiosonde and COSMIC atmospheric profile data to quantify differences among radiosonde types and the effects of imperfect collocation on comparison statistics, *J. Geophys. Res.*, 115, D23104, doi:10.1029/2010JD014457, 2010.
- Thorne, P. W., Brohan, P., Titchner, H. A., McCarthy, M. P., Sherwood, S. C., Peterson, T. C., Haimberger, L., Parker, D. E., Tett, S. F. B., Santer, B. D., Fereday, D. R., and Kennedy, J. J.: A quantification of uncertainties in historical tropical tropospheric temperature trends from radiosondes, *J. Geophys. Res.*, 116, D12116, doi:10.1029/2010JD015487, 2013.
- Trenberth, K. E.: Recent observed interdecadal climate changes in the Northern Hemisphere, *B. Am. Meteorol. Soc.*, 71, 988–993, doi:10.1175/1520-0477(1990)071<0988:ROICCI>2.0.CO;2, 1990.
- Wickert, J., Reigber, C., Beyerle, G., König, R., Marquardt, C., Schmidt, T., Grunwaldt, L., Galas, R., Meehan, T. K., Melbourne, W. G., and Hocke, K.: Atmosphere sounding by GPS radio occultation: First results from CHAMP, *Geophys. Res. Lett.*, 28, 29849–29866, doi:10.1029/2001GL013117, 2001.
- Wickert, J., Michalak, G., Schmidt, T., Beyerle, G., Cheng, C. Z., Healy, S. B., Heise, S., Huang, C. Y., Jakowski, N., Kohler, W., Mayer, C., Offiler, D., Ozawa, E., Pavlyev, A. G., Rothacher, M., Tapley, B., and Arras, C.: GPS Radio Occultation: Results from CHAMP, GRACE and FORMOSAT-3/COSMIC, *Terr. Atmos. Ocean. Sci.*, 20, 35–50, doi:10.3319/TAO.2007.12.26.01(F3C), 2009.
- Wilcox, L. J., Hoskins, B. J., and Shine, K. P.: A global blended tropopause based on ERA data – Part II: Trends and tropical broadening, *J. Geophys. Res.*, 138, 576–584, doi:10.1002/qj.910, 2011.
- WMO: Meteorology – a three-dimensional science: second session of the commission for aerology, *WMO Bulletin*, IV, 134–138, 1957.
- Zhang, M. L., Liu, L., Wan, W., and Baiqi, N.: An update global model of hmF2 from values estimated from ionosonde and COSMIC/FORMOSAT-3 radio occultation, *Adv. Space Res.*, 53, 395–402, doi:10.1016/j.asr.2013.11.053, 2014.